Chapter 3

3   THE DETERMINATION OF THE ORIENTATIONALLY UNCONSTRAINED SPATIAL MANIPULATOR WORKSPACES

3.1 INTRODUCTION

The methodology proposed for, and applied to the determination of the workspaces of *planar* mechanisms in Chapter 2 may readily be extended to apply to spatial mechanisms, such as the Stewart platforms considered by Haug et al. [12] and Liu et al. [18].

Taking the 6–3 Stewart platform of Liu et al. [18] as a representative example, the "planar" optimization approach, developed in Chapter 2, is used in this chapter to map three-dimensional workspaces of this six–DOF manipulator. The geometry of this 6–3 Stewart platform is shown in Figure 3.1.
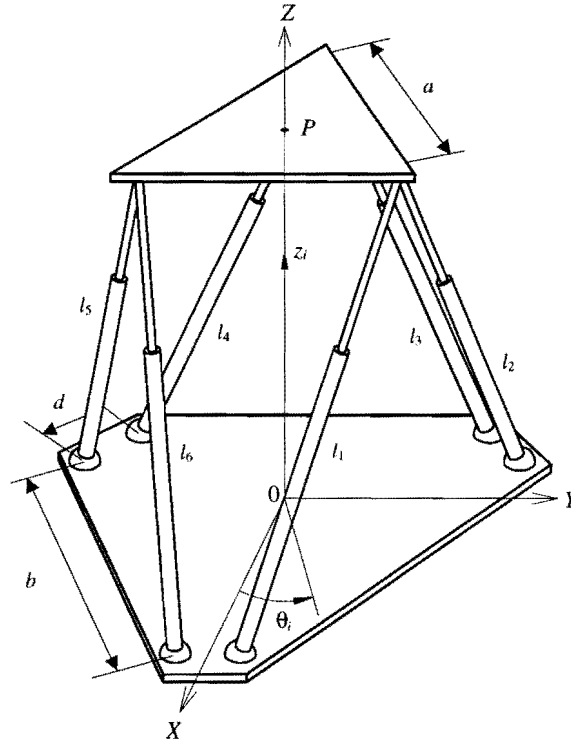

Figure 3.1 Geometry of the 6–3 Stewart platform.

The workspaces to be considered in this study are:

(i)   the orientationally unconstrained reachable workspace A, with boundary denoted by ∂A,

(ii)   the fixed orientation workspace $A\left[\alpha_{fix}, \beta_{fix}, \gamma_{fix}\right]$, with boundary indicated by $\partial A\left[\alpha_{fix}, \beta_{fix}, \gamma_{fix}\right]$, and

(iii)   an   example   of   a   dextrous   workspace $A\left[\alpha_{fix}, \beta_{fix}, \gamma_{min} - \gamma_{max}\right]$,   with   boundary

$\partial A\left[\alpha_{fix}, \beta_{fix}, \gamma_{min} - \gamma_{max}\right]$.

The corresponding different types of workspaces, (i), (ii) and (iii), were defined and determined for the planar Stewart platform considered in Section 2.6. Case (i) of the 6–3 Stewart platform is dealt with in this chapter, while cases (ii) and (iii) are dealt with in Chapter 4.

3.2 GEOMETRY OF THE 6–3 STEWART PLATFORM

As for the planar Stewart platform described in Section 2.6.1 the spatial Stewart platform also has a moving upper platform, as well as a fixed base. The base is a semi-regular hexagon, which in this case is also fixed in a horizontal position, while the upper platform is an equilateral triangle.

Figure 3.1 shows the global coordinate system fixed at the center of the base with the global Z-axes pointing vertically upwards. The working point P of the spatial Stewart platform is at the centroid of the upper triangular platform.

The spatial Stewart platform has six linear actuator legs connecting the moving upper platform, to the fixed base. The bottom ends of the actuator legs are connected to the six vertices of the base, while the top ends of the legs are connected to the three vertices of the upper platform as shown in Figure 3.1. The base platform connections are ball-and-socket (spherical) joints, while the moving platform connections are gimbals. Fichter [17] proposed these gimbals as described in Section 1.4. This arrangement is referred to as a 6–3 Stewart platform (see Section 1.4).

Varying the lengths of the linear actuators, indicated by l_i, $i = 1, 2, ..., 6$, will not only change the position of the upper platform, but also its orientation, adding up to the six DOF of the manipulator.

Adopting the definitions of Liu et al. [18], the position of the upper platform is given by the global coordinates of the working point P denoted here by (x, y, z), and the orientation of the upper platform is given by the orientation angles (α, β, γ). Liu et al. explain the orientation angles as, firstly rotating the top platform about the OX-axis through an angle α, then about the OY-axis through an angle β, and finally

about the axis radiating form the manipulator working point and fixed perpendicular to the top platform through an angle γ.

According to Liu et al. [18], the defined orientation angles have a physical meaning in that the α and β angles define an "approach vector" of the top platform, while the γ angle defines the roll of the top platform about the approach vector.

As with the planar Stewart platform, the orientationaly unconstrained reachable workspace of the spatial Stewart platform defines the *accessible* region of the working point P, and is determined by the limitations on the actuator leg lengths (see Section 2.2).

The actuator leg lengths are again the *input variables*, i.e. $\mathbf{v} = [l_1, l_2, l_3, l_4, l_5, l_6]^T$ on which the following inequality constraints, corresponding to expression (2.18) in the planar case (Section 2.6.1), are imposed:

$$0 < l_i^{min} \le l_i \le l_i^{max} \tag{3.1}$$

for $i = 1, 2, 3, ..., 6$.

Liu et al. [18] apply their kinematic analyses to an example where they propose certain dimensions for the top and bottom platforms, as well as for the actuator leg limits. In order for this example to be used for comparison purposes in the current optimization approach, the dimensions of the 6–3 Stewart platform analyzed in this chapter is in accordance with the example of Liu et al. [18].

It is important to note that, although different minimum and maximum leg length limits were prescribed for the different legs of the planar Stewart platform, here all six actuator legs of the spatial manipulator have the same leg length limits, i.e. $l_i^{min} = 8.0$ and $l_i^{max} = 15.0$ for $i = 1, 2, 3, ..., 6$. The dimensions of the top and base platforms are: $a = 10.0$, $b = 15.0$ and $d = 1.0$ (see Figure 3.1).

3.3 CONSTRAINT EQUATIONS OF THE 6–3 STEWART PLATFORM

With reference to Section 2.2, the global coordinates of the working point P on the 6–3 Stewart platform are the *output coordinates*, i.e. $\mathbf{u} = [x, y, z]^T$, and the orientation angles of the upper platform, are the *intermediate coordinates*, i.e. $\mathbf{w} = [\alpha, \beta, \gamma]^T$.

The defined input, output and intermediate coordinates of the 6–3 Stewart platform correspond to the definitions of these coordinates given in Section 2.6.2. This explains the correlation between the generalized coordinates of the spatial and planar Stewart platforms.

The spatial Stewart platform has 12 generalized coordinates compared the 6 of the planar Stewart platform. The spatial platform coordinates are:

$$\mathbf{q} = \begin{bmatrix} \mathbf{u}^\mathrm{T} & \mathbf{v}^\mathrm{T} & \mathbf{w}^\mathrm{T} \end{bmatrix}^\mathrm{T}$$
$$= \begin{bmatrix} x, & y, & z, & l_1, & l_2, ..., & l_6, & \alpha, & \beta, & \gamma \end{bmatrix}^\mathrm{T} \tag{3.2}$$

The spatial Stewart platform obviously has six degrees of freedom, and the six kinematic constraint equations of general form (2.1), are the six equations expressing the length of each leg in terms of the position and orientation coordinates. These analytical expressions can readily be found by doing the inverse kinematic analysis as described by Liu et al. [18]. These expressions, corresponding to (2.20) for the planar case, are as follows:

$$l_1 = \sqrt{\left(X_{T1} - \tfrac{d}{2\sqrt{3}} - \tfrac{b}{\sqrt{3}}\right)^2 + \left(Y_{T1} - \tfrac{d}{2}\right)^2 + Z_{T1}^2}$$

$$l_2 = \sqrt{\left(X_{T1} - \tfrac{d}{2\sqrt{3}} + \tfrac{b}{2\sqrt{3}}\right)^2 + \left(Y_{T1} - \tfrac{d}{2} - \tfrac{b}{2}\right)^2 + Z_{T1}^2}$$

$$l_3 = \sqrt{\left(X_{T2} + \tfrac{d}{\sqrt{3}} + \tfrac{b}{2\sqrt{3}}\right)^2 + \left(Y_{T2} - \tfrac{b}{2}\right)^2 + Z_{T2}^2}$$

$$l_4 = \sqrt{\left(X_{T2} + \tfrac{d}{\sqrt{3}} + \tfrac{b}{2\sqrt{3}}\right)^2 + \left(Y_{T2} + \tfrac{b}{2}\right)^2 + Z_{T2}^2} \tag{3.3}$$

$$l_5 = \sqrt{\left(X_{T3} - \tfrac{d}{2\sqrt{3}} + \tfrac{b}{2\sqrt{3}}\right)^2 + \left(Y_{T3} + \tfrac{d}{2} + \tfrac{b}{2}\right)^2 + Z_{T3}^2}$$

$$l_6 = \sqrt{\left(X_{T3} - \tfrac{d}{2\sqrt{3}} - \tfrac{b}{\sqrt{3}}\right)^2 + \left(Y_{T3} + \tfrac{d}{2}\right)^2 + Z_{T3}^2}$$

where

$$X_{T1} = x + \tfrac{a}{\sqrt{3}}\left[\sin(\alpha)\sin(\beta)\sin(\gamma+60°) + \cos(\beta)\cos(\gamma+60°)\right]$$

$$Y_{T1} = y + \tfrac{a}{\sqrt{3}}\cos(\alpha)\sin(\gamma+60°)$$

$$Z_{T1} = z + \tfrac{a}{\sqrt{3}}\left[\sin(\alpha)\cos(\beta)\sin(\gamma+60°) - \sin(\beta)\cos(\gamma+60°)\right]$$

$$X_{T2} = x - \tfrac{a}{\sqrt{3}}\left[\sin(\alpha)\sin(\beta)\sin(\gamma) + \cos(\beta)\cos(\gamma)\right]$$

$$Y_{T2} = y - \tfrac{a}{\sqrt{3}}\cos(\alpha)\sin(\gamma) \tag{3.4}$$

$$Z_{T2} = z - \tfrac{a}{\sqrt{3}}\left[\sin(\alpha)\cos(\beta)\sin(\gamma) - \sin(\beta)\cos(\gamma)\right]$$

$$X_{T3} = x + \tfrac{a}{\sqrt{3}}\left[\sin(\alpha)\sin(\beta)\sin(\gamma-60°) + \cos(\beta)\cos(\gamma-60°)\right]$$

$$Y_{T3} = y + \tfrac{a}{\sqrt{3}}\cos(\alpha)\sin(\gamma-60°)$$

$$Z_{T3} = z + \tfrac{a}{\sqrt{3}}\left[\sin(\alpha)\cos(\beta)\sin(\gamma-60°) - \sin(\beta)\cos(\gamma-60°)\right]$$

In expressions (3.3) and (3.4) a is the length of the sides of the upper equilateral triangular moving platform, and b and d are respectively the short and long sides of the hexagonal base (see Figure 3.1).

Expression (3.3) is written in standard form (2.5) as:

$$\Phi(\mathbf{u} \quad \mathbf{v} \quad \mathbf{w}) = \begin{bmatrix} v_1^2 - \left(X_{T1} - \frac{d}{2\sqrt{3}} - \frac{b}{\sqrt{3}}\right)^2 - \left(Y_{T1} - \frac{d}{2}\right)^2 - Z_{T1}^2 \\ v_2^2 - \left(X_{T1} - \frac{d}{2\sqrt{3}} + \frac{b}{2\sqrt{3}}\right)^2 - \left(Y_{T1} - \frac{d}{2} - \frac{b}{2}\right)^2 - Z_{T1}^2 \\ v_3^2 - \left(X_{T2} + \frac{d}{\sqrt{3}} + \frac{b}{2\sqrt{3}}\right)^2 - \left(Y_{T2} - \frac{b}{2}\right)^2 - Z_{T2}^2 \\ v_4^2 - \left(X_{T2} + \frac{d}{\sqrt{3}} + \frac{b}{2\sqrt{3}}\right)^2 - \left(Y_{T2} + \frac{b}{2}\right)^2 - Z_{T2}^2 \\ v_5^2 - \left(X_{T3} - \frac{d}{2\sqrt{3}} + \frac{b}{2\sqrt{3}}\right)^2 - \left(Y_{T3} + \frac{d}{2} + \frac{b}{2}\right)^2 - Z_{T3}^2 \\ v_6^2 - \left(X_{T3} - \frac{d}{2\sqrt{3}} - \frac{b}{\sqrt{3}}\right)^2 - \left(Y_{T3} + \frac{d}{2}\right)^2 - Z_{T3}^2 \end{bmatrix} = 0 \tag{3.5}$$

where

$$X_{T1} = u_1 + \tfrac{a}{\sqrt{3}}\left[\sin(w_1)\sin(w_2)\sin(w_3 + 60°) + \cos(w_2)\cos(w_3 + 60°)\right]$$

$$Y_{T1} = u_2 + \tfrac{a}{\sqrt{3}}\cos(w_1)\sin(w_3 + 60°)$$

$$Z_{T1} = u_3 + \tfrac{a}{\sqrt{3}}\left[\sin(w_1)\cos(w_2)\sin(w_3 + 60°) - \sin(w_2)\cos(w_3 + 60°)\right]$$

$$X_{T2} = u_1 - \tfrac{a}{\sqrt{3}}\left[\sin(w_1)\sin(w_2)\sin(w_3) + \cos(w_2)\cos(w_3)\right]$$

$$Y_{T2} = u_2 - \tfrac{a}{\sqrt{3}}\cos(w_1)\sin(w_3) \tag{3.6}$$

$$Z_{T2} = u_3 - \tfrac{a}{\sqrt{3}}\left[\sin(w_1)\cos(w_2)\sin(w_3) - \sin(w_2)\cos(w_3)\right]$$

$$X_{T3} = u_1 + \tfrac{a}{\sqrt{3}}\left[\sin(w_1)\sin(w_2)\sin(w_3 - 60°) + \cos(w_2)\cos(w_3 - 60°)\right]$$

$$Y_{T3} = u_2 + \tfrac{a}{\sqrt{3}}\cos(w_1)\sin(w_3 - 60°)$$

$$Z_{T3} = u_3 + \tfrac{a}{\sqrt{3}}\left[\sin(w_1)\cos(w_2)\sin(w_3 - 60°) - \sin(w_2)\cos(w_3 - 60°)\right]$$

from which in turn, given $\mathbf{u}$ and $\mathbf{w}$, one may solve for $\mathbf{v}$:

$$\mathbf{v} = \mathbf{v}(\mathbf{u}, \ \mathbf{w}) = \begin{bmatrix} \sqrt{\left(X_{T1} - \frac{d}{2\sqrt{3}} - \frac{b}{\sqrt{3}}\right)^2 + \left(Y_{T1} - \frac{d}{2}\right)^2 + Z_{T1}^2} \\ \sqrt{\left(X_{T1} - \frac{d}{2\sqrt{3}} + \frac{b}{2\sqrt{3}}\right)^2 + \left(Y_{T1} - \frac{d}{2} - \frac{b}{2}\right)^2 + Z_{T1}^2} \\ \sqrt{\left(X_{T2} + \frac{d}{\sqrt{3}} + \frac{b}{2\sqrt{3}}\right)^2 + \left(Y_{T2} - \frac{b}{2}\right)^2 + Z_{T2}^2} \\ \sqrt{\left(X_{T2} + \frac{d}{\sqrt{3}} + \frac{b}{2\sqrt{3}}\right)^2 + \left(Y_{T2} + \frac{b}{2}\right)^2 + Z_{T2}^2} \\ \sqrt{\left(X_{T3} - \frac{d}{2\sqrt{3}} + \frac{b}{2\sqrt{3}}\right)^2 + \left(Y_{T3} + \frac{d}{2} + \frac{b}{2}\right)^2 + Z_{T3}^2} \\ \sqrt{\left(X_{T3} - \frac{d}{2\sqrt{3}} - \frac{b}{\sqrt{3}}\right)^2 + \left(Y_{T3} + \frac{d}{2}\right)^2 + Z_{T3}^2} \end{bmatrix} \tag{3.7}$$

and where X_{T1}, Y_{T1}, Z_{T1}, X_{T2}, Y_{T2}, Z_{T2}, X_{T3}, Y_{T3} and Z_{T3} are given by expressions (3.6).

Finally, (2.1) may more concisely be rewritten as

$$\mathbf{v}^{min} \leq \mathbf{v} \leq \mathbf{v}^{max}$$

where $\mathbf{v}^{min}\left[l_1^{min}, l_2^{min}, ..., l_6^{min}\right]^T$ *and* $\mathbf{v}^{max}\left[l_1^{max}, l_2^{max}, ..., l_6^{max}\right]^T$ $\tag{3.8}$

and $\mathbf{v} = \mathbf{v}(\mathbf{u}, \ \mathbf{w})$ *as given by* (3.7)

Thus expressions (3.2), (3.3), (3.5), (3.7) and (3.8) here respectively correspond to (2.19), (2.20), (2.21), (2.22) and (2.23) for the planar Stewart platform.

UNIVERSITEIT VAN PRETORIA
UNIVERSITY OF PRETORIA
YUNIBESITHI YA PRETORIA

The orientationally unconstrained reachable workspace is computed with no limits on the orientation angles. As will be discussed in Chapter 4, limitations are of course imposed on the angles when the fixed orientation and dextrous workspaces are considered.

3.4 MAPPING THE ACCESSIBLE WORKSPACE OF THE 6–3 STEWART PLATFORM

3.4.1 Introduction

Two options exist by which the reachable workspace of the spatial manipulator can be mapped using the basic methodology presented for the planar accessible set (see Section 2.4).

The first option is to consider the three-dimensional workspace to be represented by a set of *horizontal* slices. For any horizontal *slice*, $z = z_i$, $i = 1, 2, ..., N_S$, the associated two dimensional workspace of the working point P may be determined in a manner analogous to that described for the planar Stewart platform in Section 2.6.2. A composite of the N_S workspace slices then yields a representation of the three-dimensional workspace.

It follows that, for a particular horizontal slice i, the boundary of the workspace ∂A_i may be mapped by solving optimization *Problem (i)* (see Section 2.3) for successive rays emanating from an interior radiating point, but now subject to an additional equality constraint:

$$u_3 = z = z_i \tag{3.9}$$

where z_i designates the height of the slice.

To complete the three dimensional representation of the workspace of the spatial Stewart platform, the boundaries ∂A_i of N_S *slices* are computed. This means that for each *slice i*, the equality constraint equation will be assigned as follows:

$$z_i = z^{\text{max}} - \frac{i}{N_S}\left(z^{\text{max}} - z^{\text{min}}\right) \tag{3.10}$$

for $i = 1, 2, ..., N_S$.

In equation (3.10), z^{min} and z^{max} are respectively the lowest and highest possible positions of the working point P measured in terms of the global coordinate system.

For each height z_i, rays emanating in the *XY*-plane from an interior radiating point will be maximized to determine the boundary ∂A_i of the workspace of *slice i*. With the global *Z*-axis pointing vertically

---

upwards from the center of the lower platform, the obvious choice for the radiating point of every *slice*, is at the fixed height z_i of that *slice*, and at the origin of the XY-plane.

Alternative to taking horizontal slices, the determination of planar workspace boundaries may also be carried out for successive vertical planes through the central axis $0Z$. This option is preferable as it avoids, to a greater extent than the first option, complications due to non-convexity. The idea is to avoid situations where two boundary points may exist for any specific search direction.

For each plane i through $0Z$, there corresponds a unique angle θ_i that the plane makes with the OX axis. For this plane the relationship $y_i/x_i = \tan\theta_i$ applies, and therefore in the optimization to determine ∂A_i for this plane, equality constraint (3.9) is replaced by

$$u_{2i} - u_{1i}\tan(\theta_i) = 0 \tag{3.11}$$

The construction of the three-dimensional reachable workspace, is carried out by determining the planar boundaries ∂A_i for a fan of N_P planes, where each plane has a different value of θ_i:

$$\theta_i = \frac{i}{N_P}\left(\frac{2\pi}{3}\right) \tag{3.12}$$

for $i = 1, 2, ..., N_P$

It is apparent from the geometry of the spatial 6–3 Stewart platform that the global Z axis is a three fold symmetry axis, and therefore it is only necessary to map a third of the complete workspace, corresponding to the θ_i range: $0° - 120°$.

For each plane the same central point, $z^0 = \left(z^{max} + z^{min}\right)/2$ on $0Z$, may be used as interior radiating point, i.e.

$$\mathbf{u}^0 = \left(0, 0, z^0\right) \tag{3.13}$$

With the dimensions of the spatial Stewart platform as given in Section 3.2, the exact coordinates of $\mathbf{u}_0$ are:

$$\mathbf{u}^0 = \left(0, 0, 7.804\right)$$

3.4.2 Computed Accessible Workspace for the 6–3 Stewart Platform

The vertical plane through the $0X$-axis ($\theta = 0°$) of the computed reachable workspace is shown in Figure 3.2

Figure 3.2 Boundaries of the accessible sets for the vertical plane through the OX-axis ($\theta = 0°$).

Apparently two different reachable boundaries seem to exist when no constraints are placed on the orientation of the top platform. As will become clear later, the inner boundary corresponds to a near global constrained local optimum solution to optimization *problem (i)*, whereas the outer boundary consists of the global maxima. These two different optima along a ray correspond to the respective maximum displacements of two different *types* of platform configurations as will be shown later.

As explained in Section 3.4.1 two options exist with which the complete accessible workspace can be mapped, namely *vertical planes*, and *horizontal slices*. Although Figure 3.2 shows the accessible sets for the vertical plane through the OX-axis ($\theta = 0°$), these results could have been obtained using both options mentioned above. The *vertical planes* option consists of a pencil of rays, restricted to the vertical plane through the OX-axis, emanating from the radiating point $\mathbf{u}^0$ at angular intervals. As for the *horizontal slices* option, Figure 3.2 can be mapped using horizontal rays, perpendicular to the OZ-axis and restricted to the vertical plane through the vertical plane through the OX-axis.

It follows that if the *horizontal slices* option is to be implemented, the highest possible and lowest possible positions of the working point have to be computed before hand to set the upper and lower

bounds between which the horizontal rays are to be incremented. The highest possible position is not a problem, as it is situated at point F on the $0Z$-axis, and can therefore easily be determined. Curve $ABCD$, however occupies a lower region than point A which is the lowest possible position of the working point if the working point is restricted to move along the $0Z$-axis. Consequently it will be difficult to implement the *horizontal slices* option, as the lower bound of the range of horizontal rays forms part of curve BC and cannot be easily determined as part of an automated process. The better option of the two, and the one used here, is the *vertical planes* option, which is easy to implement as the pencil of rays are incremented through the range $0° - 180°$.

It follows that for each ray restricted to a specific *vertical plane* and intersecting the radiating point $\mathbf{u}_0$ (3.13), a straight line relation must hold. With φ_j defined as the inclination angle between any specific ray j and the $0Z$-axis, the following equation must hold:

$$\sqrt{x_j^2 + y_j^2} - \left(z^0 - z_j\right)\tan(\varphi_j) = 0 \tag{3.14}$$

Equation (3.14) is rewritten to give the additional equality constraint needed to fix the direction of any specific ray j.

$$\sqrt{\mathbf{u}_{1j}^2 + \mathbf{u}_{2j}^2} - \left(z^0 - \mathbf{u}_{3j}\right)\tan(\varphi_j) = 0 \tag{3.15}$$

The vertical plane is covered by a pencil of N_R rays where each ray j has an inclination angle φ_j:

$$\varphi_j = \frac{j}{N_R}(\pi) \tag{3.16}$$

for $j = 0, 1, 2, ..., N_R$

Consequently, if $j = 0$, the first ray of each vertical plane will lie parallel to the $0Z$-axis, pointing in the *negative* Z-direction. The first of the two different reachable workspace boundaries in the vertical plane through the $0X$-axis, is mapped by performing an upward sweep of the radiating ray for successive inclination angles given by (3.16) and imposing equation (3.15) as additional equality constraint (see Figure 3.3).

The maximum displacement (from the radiating point $\mathbf{u}_0$) is found for successive rays $j = 1, 2, ..., N_R$, using as starting point for each optimization procedure the solution of the previous ray, $j = 0, 1, 2, ..., (N_R - 1)$. This limits the possibility of the platform "jumping" between different configurations as the rays are incremented. This procedure works well except for curve EF in Figure 3.3. The details of how curve EF is mapped, is explained in Appendix B.
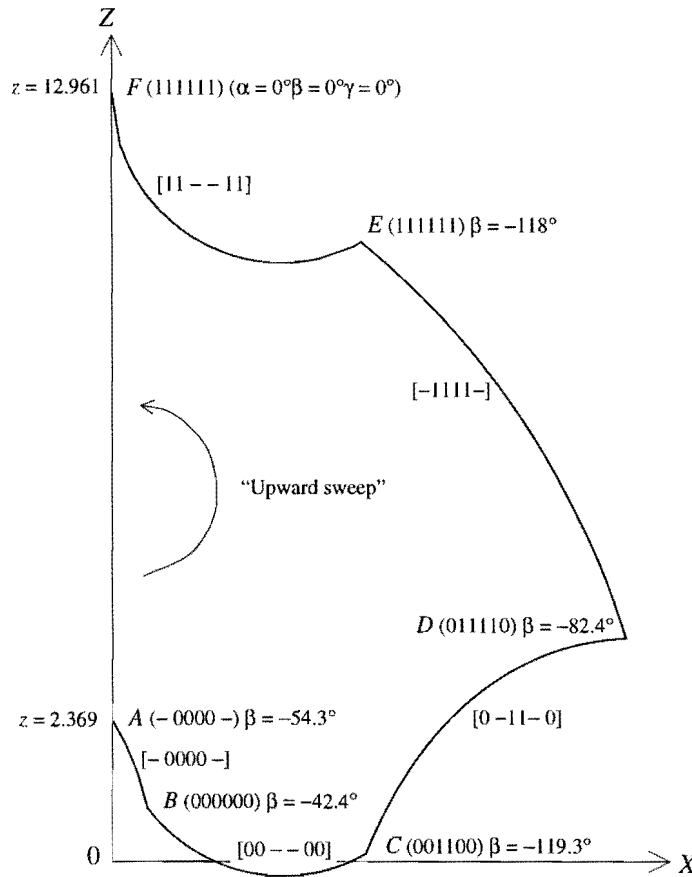
Figure 3.3 "Upward sweep" reachable workspace boundary in the vertical plane through the *OX*-axis.

Using the notation introduced in Chapter 2 and referring to Figure 3.3, the bifurcation points and boundary curves of the vertical plane through the *OX*-axis are labeled in order to differentiate between the two types of reachable boundaries that exist. The curves are now described, with the radiating ray sweeping counter clockwise upwards from the vertical, with relationship (3.15) imposed for successive ray angles φ_j given by (3.16).

The lowest possible position of the working point along the *OZ*-axis is at a height of $z = 2.369$. This is point $A\begin{pmatrix} - & 0 & 0 & 0 & 0 & - \end{pmatrix}\begin{bmatrix} 0° & -54.3° & 0° \end{bmatrix}$, which clearly is not a bifurcation point where all the actuator legs are at the specific extreme lengths.

Liu et al. [18] report that with all the actuator legs at their minimum lengths and with no platform rotation, the global coordinates of the manipulator working point are $(0, 0, 2.646)$. Using the proposed notation, this bifurcation point Liu et al. found will be labeled $\begin{pmatrix} 0 & 0 & 0 & 0 & 0 & 0 \end{pmatrix}\begin{bmatrix} 0° & 0° & 0° \end{bmatrix}$
The orientation angles of the top platform with the working point coinciding with point $A\begin{pmatrix} - & 0 & 0 & 0 & 0 & - \end{pmatrix}$ are: $\alpha = 0°$, $\beta = -54.3°$ and $\gamma = 0°$ as indicated by the notation adopted above.

The fact that β, (which measures the rotation of the top platform about the OY-axis) is the only non-zero orientation angle, indicates that actuator legs 1 and 6 have the same lengths with the working point coinciding with point $A\begin{pmatrix} - & 0 & 0 & 0 & 0 & - \end{pmatrix}$.

With the results of the optimization approach, the exact lengths of legs 1 and 6 of point $A\begin{pmatrix} - & 0 & 0 & 0 & 0 & - \end{pmatrix}$ are obtained as:

$$l_1 = l_6 = 9.759$$

Considering the above actuator leg lengths, as well as the substantial angle the top platform makes with the OY-axis ($\beta = -54.3°$), it is clear that the upper platform is in a "flipped" orientation at point $A\begin{pmatrix} - & 0 & 0 & 0 & 0 & - \end{pmatrix}$. Although this is a mathematically feasible orientation, mechanically it may not be possible due to the actuator legs interfering with each other, and the limited rotations of the joints connecting the legs with the base and moving platform.

Purely mathematically, the working point of the "flipped" top platform advances along boundary curve $AB\begin{bmatrix} - & 0 & 0 & 0 & 0 & - \end{bmatrix}$ until it reaches bifurcation point $B\begin{pmatrix} 0 & 0 & 0 & 0 & 0 & 0 \end{pmatrix}$, where all the actuator legs take on their minimum lengths, and the orientation angles of the top platform are: $\alpha = 0°$, $\beta = -42.4°$ and $\gamma = 0°$.

The top platform remains in its flipped orientation as the working point advances from bifurcation point $B\begin{pmatrix} 0 & 0 & 0 & 0 & 0 & 0 \end{pmatrix}$ along curves $BC\begin{bmatrix} 0 & 0 & - & - & 0 & 0 \end{bmatrix}$, $CD\begin{bmatrix} 0 & - & 1 & 1 & - & 0 \end{bmatrix}$ and $DE\begin{bmatrix} - & 1 & 1 & 1 & 1 & - \end{bmatrix}$. It is interesting to note that the extreme bifurcation points B $\begin{pmatrix} 0 & 0 & 0 & 0 & 0 & 0 \end{pmatrix}$, and $E\begin{pmatrix} 1 & 1 & 1 & 1 & 1 & 1 \end{pmatrix}$ are asymmetrically placed off the OZ-axis. With the manipulator working point coinciding with bifurcation point $E\begin{pmatrix} 1 & 1 & 1 & 1 & 1 & 1 \end{pmatrix}$, the top platform is in an extreme flipped orientation ($\alpha = 0°$, $\beta = -118°$ and $\gamma = 0°$), which explains the existence of curve $EF\begin{bmatrix} 1 & 1 & - & - & 1 & 1 \end{bmatrix}$. Starting in the flipped orientation ($\beta = -118°$) at bifurcation point E $\begin{pmatrix} 1 & 1 & 1 & 1 & 1 & 1 \end{pmatrix}$, curve EF denotes the path along which actuator legs 3 and 4 are retracted until the top platform is out of this flipped configuration. Actuator legs 3 and 4 are then extended again as the working point advances along the rest of the curve $EF\begin{bmatrix} 1 & 1 & - & - & 1 & 1 \end{bmatrix}$ and eventually reaches bifurcation point $F\begin{pmatrix} 1 & 1 & 1 & 1 & 1 & 1 \end{pmatrix}$ where the top platform is horizontally orientated ($\alpha = 0°$, $\beta = 0°$ and $\gamma = 0°$). This completes the upward sweep of the radiating ray.

Point F $(1 \quad 1 \quad 1 \quad 1 \quad 1 \quad 1)$ is at a height of $z = 12.961$ which corresponds to Liu et al.'s [18] reported global coordinates of the manipulator working point $(0, \ 0, \ 12.96)$, when all the actuator legs are at their maximum lengths.

Following the upward sweep the mapping may be continued by initiating a subsequent downward sweep. It follows that equation (3.14) can be changed so that the rays for any specific vertical plane are incremented starting with the initial ray parallel to the *positive* Z-direction and incrementing φ_j through $180°$ ending with the final ray parallel to the *negative* Z-direction. Constraint equation (3.14) now becomes:

$$\sqrt{x_j^2 + y_j^2} - (z_j - z^0)\tan(\varphi_j) = 0 \qquad (3.17)$$

Which can once again be rewritten in terms of the generalized coordinates to give:

$$\sqrt{u_{1j}^2 + u_{2j}^2} - (u_{3j} - z^0)\tan(\varphi_j) = 0 \qquad (3.18)$$

The reachable workspace in the vertical plane through the OX-axis is now re-mapped using equality (3.18) instead of (3.15), and incrementing φ_j as given by expression (3.16), resulting in a downward sweep of the radiating ray.

Here again the maximum displacements of the respective rays $j = 1, 2, ..., N_R$ are found using as starting point for the successive optimizations, the solution for the previous ray, $j = 0, 1, 2, ..., (N_R - 1)$.

Figure 3.4 shows the re-mapped reachable workspace boundary in the vertical plane through the OX-axis ($\theta_i = 0°$). Starting from bifurcation point F $(1 \quad 1 \quad 1 \quad 1 \quad 1 \quad 1)$ where the top platform is horizontally orientated ($\alpha = 0°$, $\beta = 0°$ and $\gamma = 0°$), the working point advances along the curve FG $[- \quad 1 \quad 1 \quad 1 \quad 1 \quad -]$ as the platform moves away from the OZ-axis. Although curve FG $[- \quad 1 \quad 1 \quad 1 \quad 1 \quad -]$ in Figure 3.4 carries the same label as curve DE $[- \quad 1 \quad 1 \quad 1 \quad 1 \quad -]$ in Figure 3.3, the two boundary curves do not coincide as is evident from the earlier composite Figure 3.2. The reason for this is that the top platform is now positively tilted as the working point advances along curve FG $[- \quad 1 \quad 1 \quad 1 \quad 1 \quad -]$ in Figure 3.4, while the top platform is in a negatively flipped orientation as the working point advances along curve DE $[- \quad 1 \quad 1 \quad 1 \quad 1 \quad -]$ in Figure 3.3. The positively tilted orientation of the top platform is $\alpha = 0°$, $\beta = 31.9°$ and $\gamma = 0°$ when the manipulator working point coincides with bifurcation point G $(0 \quad 1 \quad 1 \quad 1 \quad 1 \quad 0)$ in Figure 3.4.
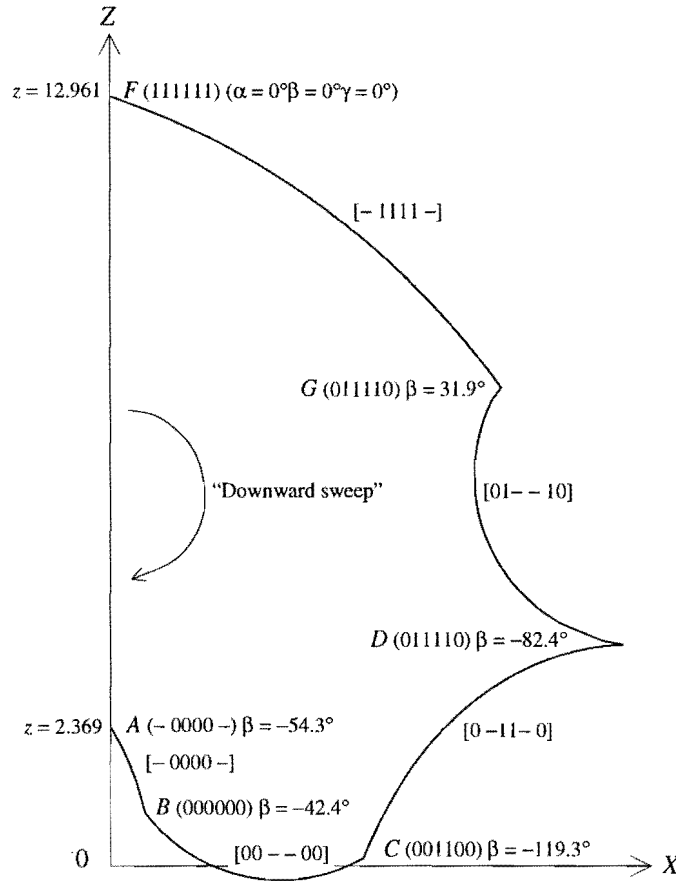
Figure 3.4 "Downward sweep" reachable workspace boundary in the vertical plane through the OX-axis $(\theta = 0°)$.

The "downward sweep" re-mapped reachable boundary in Figure 3.4 shows a boundary curve GD $\begin{bmatrix} 0 & 1 & - & - & 1 & 0 \end{bmatrix}$ between bifurcation points $G(0 \quad 1 \quad 1 \quad 1 \quad 1 \quad 0)$ and $D(0 \quad 1 \quad 1 \quad 1 \quad 1 \quad 0)$. The behavior along curve GD $\begin{bmatrix} 0 & 1 & - & - & 1 & 0 \end{bmatrix}$ in Figure 3.4 is similar to that along curve EF $\begin{bmatrix} 1 & 1 & - & - & 1 & 1 \end{bmatrix}$ in Figure 3.3. Starting at bifurcation point $G(0 \quad 1 \quad 1 \quad 1 \quad 1 \quad 0)$, actuator legs 3 and 4 are retracted as the manipulator working point advances along the first portion of curve GD $\begin{bmatrix} 0 & 1 & - & - & 1 & 0 \end{bmatrix}$. This action forces the top platform from the positively tilted orientation at bifurcation point $G(0 \quad 1 \quad 1 \quad 1 \quad 1 \quad 0)$ ($\alpha = 0°$, $\beta = 31.9°$ and $\gamma = 0°$), into the negatively flipped orientation ($\alpha = 0°$, $\beta = -82.36°$ and $\gamma = 0°$) with the manipulator working point coinciding with bifurcation point D $(0 \quad 1 \quad 1 \quad 1 \quad 1 \quad 0)$. The manipulator working point follows the last portion of curve GD $\begin{bmatrix} 0 & 1 & - & - & 1 & 0 \end{bmatrix}$ as actuator legs 3 and 4 are extended, so that these legs take on their maximum leg lengths when bifurcation point D $(0 \quad 1 \quad 1 \quad 1 \quad 1 \quad 0)$ is reached.

Comparing Figure 3.3 with Figure 3.4 shows, as is also apparent from the composite Figure 3.2, that the bottom portion of the mapped reachable boundary is the same independent of whether the upward sweep or downward sweep mapping is done.

Looking at the results obtained, it is evident that the reachable workspace is characterized by different boundary curves corresponding to different types of orientations of the top platform. More specifically, analyzing the reachable boundary in the vertical plane through the OX-axis, shows that the negatively flipped orientation is *not* mechanically feasible at all positions where the mathematical solution exists.

Although the computation of the workspace was restricted here to the plane through the OX-axis $(\theta = 0°)$, it may be done in a straight forward similar manner for any other vertical plane through OZ, i.e. for any other θ value.

The demonstration of the successful mapping of the workspace in the vertical plane through the OX-axis proves that the optimization approach adopted here is a tool with which the mathematically complete reachable workspace can be mapped. The mapping of such a complete workspace is of course of limited practical use if it encloses mechanically infeasible regions. However, if the spherical and gimbal joint limits are taken into consideration, and the actuator legs are prohibited to interfere while mapping the reachable workspace, the complete workspace will be mechanically feasible and of practical value. These aspects will be addressed in the future research envisaged and is also discussed in more detail in Chapter 5.

In the next chapter the complete fixed orientation workspace $A\left[\alpha_{fix}, \beta_{fix}, \gamma_{fix}\right]$, with boundary $\partial A\left[\alpha_{fix}, \beta_{fix}, \gamma_{fix}\right]$, as well as an example of a complete dextrous workspace $A\left[\alpha_{fix}, \beta_{fix}, \gamma_{min} - \gamma_{max}\right]$, with boundary $\partial A\left[\alpha_{fix}, \beta_{fix}, \gamma_{min} - \gamma_{max}\right]$ are determined.